Published in final edited form as:
Carbon N Y. 2011 October 1; 49(12): 3789–3795. doi:10.1016/j.carbon.2011.04.070.

The production of oxygenated polycrystalline graphene by one-step ethanol-chemical vapor deposition

Rajat K. Paul[*,†,‡], **Sushmee Badhulika**[‡], **Sandip Niyogi**[§,⊥], **Robert C. Haddon**[§,⊥], **Veera M. Boddu**[#], **Carmen Costales-Nieves**[#], **Krassimir N. Bozhilov**[‖], and **Ashok Mulchandani**[*,§,⊥]

[†]Department of Mechanical Engineering, University of California, Riverside, CA 92521, USA

[‡]Department of Electrical Engineering, University of California, Riverside, CA 92521, USA

[§]Department of Chemistry, University of California, Riverside, CA 92521, USA

[⊥]Chemical and Environmental Engineering and Center for Nanoscale Science and Engineering, University of California, Riverside, CA 92521, USA

[‖]Central Facility for Advanced Microscopy and Microanalysis, University of California, Riverside, CA 92521, USA

[#]US Army Engineer Research and Development Center and Construction Engineering Research Laboratory, Champaign, IL 61822, USA

Abstract

Large-area mono- and bilayer graphene films were synthesized on Cu foil (~ 1 inch^2) in about 1 min by a simple ethanol-chemical vapor deposition (CVD) technique. Raman spectroscopy and high resolution transmission electron microscopy revealed the synthesized graphene films to have polycrystalline structures with 2–5 nm individual crystallite size which is a function of temperature up to 1000°C. X-ray photoelectron spectroscopy investigations showed about 3 atomic% carboxylic (COOH) functional groups were formed during growth. The field-effect transistor devices fabricated using polycrystalline graphene as conducting channel (L_c=10 μm; W_c=50 μm) demonstrated a p-type semiconducting behavior with high drive current and Dirac point at ~35 V. This simple one-step method of growing large area polycrystalline graphene films with semiconductor properties and easily functionalizable groups should assist in the realization of potential of polycrystalline graphene for nanoelectronics, sensors and energy storage devices.

1. Introduction

Graphene, a one atom thick sp^2-hybridized two-dimensional (2D) honeycomb lattice of a carbon allotrope, because of its unique band structure, band-tuning ability, extremely high carrier mobility, themal transport properties and high chemical stability [1–3], is being envisioned as a promising material for replacing silicon in future electronics towards applications in actuators, solar cells, field-emission devices, field-effect transistors, supercapacitors, and batteries [4–9]. To realize this goal will require large area synthesis of high quality graphene layers that is not presently possible with the current exfoliation method.

Among the several approaches reported to-date, chemical vapor deposition (CVD) of carbon atoms on metal substrates has created great interest because of the low-cost production of graphene layers [10, 11]. Most importantly, highly crystalline large area monolayer

[*]Corresponding author: Tel: 951-827-6419 adani@engr.ucr.edu (A. Mulchandani). [*]rpaul003@ucr.edu (R. K. Paul).

graphene film can be grown directly on a copper (Cu) surface by a surface-catalysis process up to 1000°C using a gaseous or solid carbon source such as methane (CH_4), acetylene (C_2H_2) and polymethaylmethacrylate (PMMA) without the limitation of the underlying features of the copper substrate [6, 10, 12, 13]. Perfectly crystalline graphene, a zero bandgap material, while ideal for several electronic applications, lacks the semiconductor properties required for application as a transistor channel. Development of bandgap energy in graphene has ranged from lateral charge confinement in lithographically patterned graphene nanoribbons to covalent attachment of aryl groups to the basal carbon and doping with nitrogen [14–16].

A recent report on electronic transport modeling in polycrystalline graphene showed that an introduction of a short-range charge disorder, that is about 0.1 nm^{-1}, can help achieve a higher on/off current ratio of about 10^3 larger than that of top gated single crystalline monolayer graphene field-effect transistor (about 5) [17, 18]. In fact, an introduction of a controlled amount of crystal defects could be a band-tuning tool for semi-metallic graphene film without engaging bulk bandgaps to achieve desired electronic properties. However, in a typical graphene synthesis method, incorporation of randomly oriented defects in the form of polycrystallinity should be the common features in the graphene film instead of having a certain periodicity of defects. Thus, a disorder induced polycrystalline graphene film may be worth studying in its practical application in nano- and opto-electronics.

In this report, we have evaluated the use of ethanol vapor as a carbon source for the synthesis of large area (>1 sq. in.) graphene by CVD on copper foil. Detailed investigation of the mono- and bi-layer graphene synthesized by ethanol precursor for 1 min by Raman spectroscopy, high resolution transmission electron microscopy (HRTEM), X-ray photoelectron spectroscopy (XPS) revealed the material to be polycrystalline with a large number of edge defects and disorder and C=O and COOH groups. The size of graphene nanocrystal in the polycrystalline graphene, the amount of oxygen-related groups and the amount of sp^2- and sp^3-hybridized carbon were a function of the synthesis temperature. Field-effect transistor investigations demonstrated the film to be a p-type semiconductor with high drive current capacity. Randomly oriented defects towards the grain boundaries of polycrystalline graphene could be beneficial to incorporate specific doping elements and/or different functional groups in the defect sites to achieve desired electronic properties.

2. Experimental

2.1 Growth and transfer of polycrystalline graphene

Graphene films were grown by CVD process on copper foil (25 μm thick and 2.5 cm × 2.5 cm) as growth substrate. The process started with cleaning of the foil with acetone followed by drying with blowing Ar gas. The foil was then placed inside a fused silica tube (5 cm inside diameter by 100 cm long) and the temperature raised to 1000°C under flowing Ar/H_2, 200 sccm (standard cubic centimeter per min)/100 sccm, followed by annealing for 30 min. The flow rates were controlled precisely by mass flow controllers. Graphene was synthesized at the specified growth temperature under an atmosphere of ethanol vapors in Ar as carrier gas (200 sccm) by the bubbling of anhydrous ethanol and H_2 at 100 sccm for 1 min. After the reaction the bubbling was stopped and the substrate cooled naturally down to room temperature under Ar/H_2 flow. Bilayer graphene films were removed from the Cu foil by etching in a 1 M aqueous $FeCl_3$ solution, followed by subsequent cleaning with an aqueous HCl (5%) and D.I. water. The cleaning steps were performed by gently removing the solution several times using a pipette to keep the graphene flims intact on the D.I. water surface. For monolayer, graphene on one side of Cu foil was removed with O_2 plasma before the etching of the foil. Graphene film was transferred/collected onto quartz or SiO_2/Si substrate by contacting the substrate with the film floating on water. In the case of CH_4-

CVD of graphene film, the growth was performed at 900°C for 5 min in flowing $Ar/H_2/CH_4$ (200/100/10 sccm) atmosphere.

2.2 Materials characterization

Detailed characterization of synthesized large-area graphene layer was performed using optical microscopy, Raman spectroscopy (Nicolet Almega XR Raman microscope; λ_{EX}=532 nm), X-ray photoelectron spectroscopy (XPS; PHI Model 5400AXIS Ultra Kratos XPS) and transmission electron microscopy (TEM; Philips, CM300, Japan) with a LaB6 cathode operated at 300kV.

For electrical characterization, the as-grown graphene film was transferred on p+ Si/SiO_2 substrate. The heavily doped Si substrate served as a global back-gate, while the thermally grown SiO_2 (300 nm) was used as gate insulator. Source and drain electrodes were fabricated to a graphene film (channel length, Lc: 10 μm and width, Wc: 50 μm) using photolithography to define the contact areas, followed by electron-beam evaporation of Cr (20 nm)/Au (180 nm) using an E-beam evaporator (Temescal, BJD-1800). I–V characteristics of individual graphene FET were obtained at room temperature using a semiconductor parameter analyzer (Hewlett Packard-4155A, Austin, TX, USA).

3. Results and discussion

Fig. 1a shows optical micrographs of mono and bilayer polycrystalline graphene films grown at 900°C for 1 min in flowing H_2 (80 sccm) and ethanol vapor saturated Ar (200 sccm) atmospheres, floating on deionized (D.I.) water after etching of Cu foil in 1 M aqueous $FeCl_3$ solution. Since graphene was formed on both sides of the Cu foil (~25 μm thick), two films are attached together on the removal of interfacial Cu foil during the etching process to give a bilayer. For monolayer graphene, one side of the Cu foil was exposed to O_2 plasma to extract the film formed on the other side. Both monolayer and bilayer films had high transparencies as evident by 97% and 91% transmittance, respectively, in the 500 to 1000 nm wavelength regime (Fig. 1b).

The Raman spectrum of single layer graphene films synthesized using ethanol vapor and CH_4 precursors at 900°C are presented in Fig. 2a. As expected, the Raman spectrum of graphene film grown using CH_4 precursor had (a) G-band (1560 cm^{-1} to 1620 cm^{-1}) comprised of E2g vibrational mode of sp^2-bonded carbon in a two dimensional hexagonal lattice, (b) a negligible disorder mode D-band (1300 cm^{-1} to 1400 cm^{-1}) due to the breathing vibrations of sp^2 carbon rings with dangling bonds in plane terminations of the disordered graphite which becomes Raman active after neighboring sp^2 carbons are converted to sp^3 hybridization in graphitic structure [19, 20], (c) 2D-band (2660 cm^{-1} to 2700 cm^{-1}) comprised of a second order vibration appearing from the scattering of phonons at the zone boundary and (d) 2D-band intensity approximately two times the intensity of G-band. These results are consistent with the characteristics for highly crystalline graphene layers [10, 11]. On the other hand, in the case of graphene film grown using ethanol vapor the intensity of D-band at 1345 cm^{-1} became the most prominent feature in the Raman spectrum and the characteristic 2D-band intensity at 2675 cm^{-1} was significantly reduced, characteristics of highly disordered sp^3 hybridization of carbon lattice was not observed in graphene film synthesized using CH_4. Further, these films had a large number of edge defects and disorder as evidenced by the well-defined presence of D* band at 1620 cm^{-1} and strong (G + D) band at about 2940 cm^{-1}, respectively [21].

Having confirmed that the graphene film using ethanol vapor had unique polycrystalline features not present in methane grown film, we investigated the effect of synthesis temperature, while keeping the other process parameters constant, on crystallinity using

Raman microscopy (Fig. 2b–e). As shown in these spectra, the FWHM (full width at half maximum) of the G-band decreased and was an inverse function of the growth temperature, which is direct evidence of enhanced sp^2-hybridization of carbon lattice and the annealing of structural defects [22]. On the other hand, the I_D/I_G ratio decreased gradually from a value of 1.36 at 850°C (Fig. 2b) to about 0.38 at 1000°C (Fig. 2e), revealing the restoration of damaged lattice, i.e., induction of the crystalline order at higher growth temperature. However, the presence of disorder-induced D and (G+D) features in the graphene film synthesized by ethanol-CVD was not totally diminished even up to 1000 °C. Thus, the higher growth temperature may increase the crystallite size in polycrystalline graphene film only by the maximal restoration of existing defects up to 1000 °C, which were further analyzed using TEM studies (Figs. 3 and 4). This observation confirms the existence of short-range order in graphene films even at higher growth temperatures as well as the inability of these films to achieve long range order of AB stacking sequences.

Fig. 3 shows a comparison of the electron diffraction patterns taken from the graphene films synthesized at 900°C using ethanol vapor and CH_4 gas. The ethanol-derived graphene film (Fig. 3a) consisted of concentric rings corresponding to (002) and (100) planes of graphitic structures, which are expected due to the highly polycrystalline nature of the graphene layer. The Bragg spacings d_{002} and d_{100} were found to be 0.347 nm and 0.210 nm as compared to 0.348 nm and 0.212 nm, respectively, for single crystal graphitic structure (JCPDS data). On the other hand, the CH_4-derived graphene film (Fig. 3b) had the typical six-fold symmetrical spots attributed to the long range crystalline ordering of mono- or bi-layer single crystal graphene film.

To further characterize the polycrystallinity in ethanol-derived graphene film, HRTEM analysis was carried out. Fig. 4 shows HRTEM and corresponding inverted FFT images of graphene films synthesized at 900°C and 1000°C for 1 min using ethanol vapor. The size of individual crystals in polycrystalline graphene synthesized at 900°C and 1000°C were about ~2 nm (Fig. 4c) and ~5 nm (Fig. 4d), respectively. The inset HRTEM image in Fig. 4b clearly shows the two dimensional lattice fringes of individual graphene crystals. The interplanar d-spacing measured from the fringe pattern, as indicated in Fig. 4b, was about 0.215 nm corresponding to the {100} planes of the graphitic crystal system. These results revealed that the size of graphene nanocrystals in the polycrystalline graphene film increased at 1000°C due to the restoration of defect sites at high temperature.

Fig. 5 shows the X-ray photoelectron spectroscopy (XPS) of graphene films grown by ethanol-CVD at 900°C and 1000°C. We first examined the XPS spectra for graphene synthesized at 900°C. As shown in Fig. 5a, the C 1s XPS spectra exhibited three Gaussian peaks centered at 284.2 eV, 285.5 eV and 288.3 eV, attributed to sp^2-hybridized carbon atoms (C=C), keto (C=O) and carboxylic (COOH) or epoxy groups, respectively [21, 23]. The presence of C=O and COOH are strong indicators of considerable degree of oxidation. The amount of sp^2- and sp^3-hybridized carbon were estimated to be 92% and 8%, respectively. The ratio of sp^3/sp^2 carbon atoms could also explain the large intensity of the D-band observed in Raman spectroscopy in Fig. 2. It is likely that oxygen-related functional groups could have originated from the dissociated ethanol vapor at high temperature. The grain boundaries in polycrystalline graphene are unsaturated carbon sites where bound oxygen and hydrogen in the oxygen related functional groups could saturate the carbon dangling bonds. The amount of –COOH functional group was estimated at ~3 atomic%, which is comparable to the 0.5 to 3% in commercial CNTs. The high content of COOH functional groups in the large area polycrystalline graphene were incorporated in-situ during the CVD growth as opposed to the traditional post-synthesis nitric acid refluxing, as in the case of CNTs. This is a significant advantage since acid treatement involves modification of unsaturated carbon-carbon bonds on CNT surfaces that can have serious implications on

electronic properties. The presence of COOH groups opens the way for further functionalization and covalent binding of various monomer and polymer matrices to graphene for applications in energy storage, biological systems, photovoltaics and nanoelectronics [22–24]. Further studies would be required for a better understanding of methods to control the amount of functional groups in the polycrystalline graphene. Figure 5b shows the XPS spectra of polycrystalline graphene film synthesized at 1000°C. While spectra were similar in terms of the major peaks, there were however subtle important differences. Notably, there was an increase in the intensity and sharpness of the peak at 284.6 eV and decrease in the intensity of the peak at 288.3 eV. The former is attributed to increased sp^2-hybridization of carbon lattice at higher temperatures whereas the latter is a result of the removal of oxygen-related functional groups during cooling of the film from 1000°C to room temprature under Ar/H_2 environment. The amount of sp^2- and sp^3-hybridized carbon atoms were estimated at about 97% and 3%, respectively, compared to 92% and 8%, respectively, in film grown at 900°C (Fig. 5a). Moreover, there was a typical redshift (~0.4 eV) towards lower binding energy and broadening of C 1s peaks caused by the incorporation of oxide functional groups which is similar to the case for p-doped carbon nanotubes in graphene film synthesized at 900°C compared to one synthesized at 1000°C [25,26].

To evaluate the impact/contribution of oxide functional group incorporation on the electronic properties of polycrystalline graphene film, we performed field-effect transistor studies (Fig. 6), on polycrystalline graphene having channel length (L_c) and width (W_c) of about 10 μm and 50 μm, respectively. Source-drain current (I_{ds}) vs. the source-drain voltage (V_{ds}) characteristic curves at different gate voltages (V_g) for the polycrystalline graphene (Fig. 6a) exhibited typical p-channel transistor behavior as well as clear gate modulation of conductance compared with that of CH_4-CVD grown graphene film, which could be attributed to the polycrystalline nature of ethanol-CVD grown graphene film [11]. Additionally, the total drive current of the polycrystalline graphene FET showed comparatively much higher value than the sub-micron width bulk graphene FET showing similar gate modulation with the gate biases [10, 11, 15]. Similarly, the transfer curve of the device with back gate voltage varied from −40 to 40 V at V_{ds} of 1V showed a slow increase of I_{ds} with decreasing V_g (Fig. 6b), confirming a p-type behavior of the polycrystalline graphene FET having a Dirac point at about 35V. The p-type behavior as well as shifting of the Dirac point can also be attributed to the adsorbed oxygen and the oxygen-related functional groups (such as C=O and COOH) and is in accordance with the observations of p-type doping when the edge defects in carbon nanotube (CNT), CVD graphene and graphene nanoribbon are terminated by hydrogen and oxygen and hydroxyl and carboxylic groups [27–29]. The decrease in L_c and W_c of polycrystalline graphene channel by patterning polycrystalline graphene into nanoribbons 30–32] or nanomesh [33] can potentially improve gate modulation further.

4. Summary

Using an ethanol-chemical vapor deposition technique, polycrystalline graphene film was synthesized utilizing surface catalysis mechanism on a copper surface. By using Raman spectroscopy, X-ray photoelectron spectroscopy, electron diffraction pattern analysis and high-resolution transmission electron microscopy techniques, we demonstrated the polycrystalline nature of synthesized graphene film showing p-type semiconducting behavior as well as incorporation of oxygen-related carboxylic functional group (~ 3 at.%). The sizes of individual graphene crystallite in the graphene films synthesized at 900°C and 1000°C were about 2 nm and 5 nm, respectively, and they are oriented in [100] the crystal direction. The synthesized polycrystalline graphene film could potentially be exploited in the doping of heteroatoms as well as binding with other functional groups for desired

applications. The reported method provides large-area polycrystalline graphene film, which could be a potential candidate to study further for applications in sensors, energy storage, biological systems and nanoelectronics.

Acknowledgments

We acknowledge the financial support from the Dean of Bourns College of Engineering at the University of California, Riverside and the National Institutes of Health grant U01ES016026. Part of the characterization work was carried out in the Frederick Seitz Materials Research Laboratory Central Facilities, University of Illinois, which are partially supported by the U.S. Department of Energy under grants DE-FG02-07ER46453 and DE-FG02-07ER46471.

References

1. Novoselov KS, Geim AK, Morozov SV, Jiang D, Zhang Y, Dubonos SV, et al. Electric field effect in atomically thin carbon films. Science. 2004; 306:666–669. [PubMed: 15499015]
2. Zhang Y, Tan JW, Stormer HL, Kim P. Experimental observation of the quantum Hall effect and Berry's phase in graphene. Nature. 2005; 438:201–204. [PubMed: 16281031]
3. Novoselov KS, Geim AK, Morozov SV, Jiang D, Katsnelson MI, Grigorieva IV, et al. Two-dimensional gas of massless Dirac fermions in graphene. Nature. 2005; 438:197–200. [PubMed: 16281030]
4. Lin J, Penchev M, Wang G, Paul RK, Zhong J, Jing X, et al. Heterogeneous graphene nanostructures: ZnO nanostructures grown on large-area graphene layers. Small. 2010; 6:2448–2452. [PubMed: 20878792]
5. Wang X, Zhi L, Mullen K. Transparent, conductive graphene electrodes for dyesensitized solar cell. Nano Lett. 2008; 8:323–327. [PubMed: 18069877]
6. Paul RK, Ghazinejad M, Penchev M, Lin J, Ozkan M, Ozkan CS. Synthesis of a pillared graphene nanostructure: a counterpart of three-dimensional carbon architectures. Small. 2010; 6:2309–2313. [PubMed: 20862676]
7. Yoo E, Kim J, Hosono E, Zhou H, Kudo T, Honma I. Large reversible Li storage of graphene nanosheet families for use in rechargeable lithium ion batteries. Nano Lett. 2008; 8:2277–2282. [PubMed: 18651781]
8. Blake P, Brimicombe PD, Nair RR, Booth TJ, Jiang D, Schedin F, et al. Graphene-based liquid crystal device. Nano Lett. 2008; 8:1704–1708. [PubMed: 18444691]
9. Nair RR, Blake P, Grigorenko AN, Novoselov KS, Booth TJ, Stauber T, et al. Fine structure constant defines visual transparency of graphene. Science. 2008; 320:1308. [PubMed: 18388259]
10. Li X, Cai W, An J, Kim S, Nah J, Yang D, et al. Large-area synthesis of high-quality and uniform graphene films on copper foils. Science. 2009; 324:1312–1314. [PubMed: 19423775]
11. Kim KS, Zhao Y, Jang H, Lee SY, Kim JM, Kim KS, et al. Large-scale pattern growth of graphene films for stretchable transparent electrodes. Nature. 2009; 457:706–710. [PubMed: 19145232]
12. Sun Z, Yan Z, Yao J, Beitler E, Zhu Y, Tour JM. Growth of graphene from solid carbon sources. Nature. 2010; 468:549–552. [PubMed: 21068724]
13. Rasool HI, Song EB, Allen MJ, Wassei JK, Kaner RB, Wang KL, et al. Continuity of graphene on polycrystalline copper. Nano Lett. 2011; 11:251–256. [PubMed: 21117698]
14. Niyogi S, Bekyarova E, Itkis ME, Zhang H, Shepperd K, Hicks J, et al. Spectroscopy of covalently functionalized graphene. Nano Lett. 2010; 10:4061–4066. [PubMed: 20738114]
15. Wei D, Liu Y, Wang Y, Zhang H, Huang L, Yu G. Synthesis of n-doped graphene by chemical vapor deposition and its electrical properties. Nano Lett. 2009; 9:1752–1758. [PubMed: 19326921]
16. Bekyarova E, Itkis ME, Ramesh P, Berger C, Sprinkle M, deHeer WA, et al. Chemical modification of epitaxial graphene: spontaneous grafting of aryl groups. J Am Chem Soc. 2009; 131:1336–1337. [PubMed: 19173656]
17. Kim P. Graphene: across the border. Nat Mater. 2010; 9:792–793. [PubMed: 20864938]
18. Yazyev OV, Louie SG. Electronic transport in polycrystalline graphene. Nat Mater. 2010; 9:806–809. [PubMed: 20729847]

19. Ferrari AC, Meyer JC, Scardaci V, Casiraghi C, Lazzeri M, Mauri F, et al. Raman spectrum of graphene and graphene layers. Phys Rev Lett. 2006; 97:187401–187404. [PubMed: 17155573]
20. Malard LM, Pimenta MA, Dresselhaus G, Dresselhaus MS. Raman spectroscopy in graphene. Phys Rep. 2009; 473:51–87.
21. Campos-Delgado J, Romo-Herrera JM, Jia X, Cullen DA, Muramatsu H, Kim YA, et al. Bulk production of a new form of sp^2 carbon: crystalline graphene nanoribbons. Nano Lett. 2008; 8:2773–2778. [PubMed: 18700805]
22. Dresselhaus M, Jorio SA, Saito R. Characterizing graphene, graphite, and carbon nanotubes by Raman spectroscopy. Annu Rev Condens Matter Phys. 2010; 1:89–108.
23. Campos-Delgado J, Farhat H, Kim YA, Reina A, Kong J, Endo M, et al. Resonant Raman study on bulk and isolated graphitic nanoribbons. Small. 2009; 5:2698–2702. [PubMed: 19821454]
24. Janowska I, Chizari K, Ersen O, Zafeiratos S, Soubane D, Costa VD, et al. Microwave synthesis of large few-layer graphene sheets in aqueous solution of ammonia. Nano Res. 2010; 3:126–137.
25. Bae S, Kim H, Lee Y, Xu X, Park JS, Zheng Y, et al. Roll-to-roll production of 30-inch graphene films for transparent electrodes. Nat Nanotechnol. 2010; 5:574–578. [PubMed: 20562870]
26. Geng HZ, Kim KK, So KP, Lee YS, Chang Y, Lee YH. Effect of acid treatment on carbon nanotube-based flexible transparent conducting films. J Am Chem Soc. 2007; 129:7758–7759. [PubMed: 17536805]
27. Woo HS, Czerw R, Webster S, Carroll DL, Ballato J, Strevens AE, et al. Hole blocking in carbon nanotube-polymer composite organic light-emitting diodes based on poly (m-phenylene vinylene-co-2, 5-dioctoxy-p-phenylene vinylene). Appl Phys Lett. 2000; 77:1393–1395.
28. Gunlycke D, Li J, Mintmire JW, White CT. Altering low-bias transport in zigzag-edge graphene nanostrips with edge chemistry. Appl Phys Lett. 2007; 91:112108–112110.
29. Wang X, Li X, Zhang L, Yoon Y, Weber PK, Wang H, et al. N-doping of graphene through electrothermal reactions with ammonia. Science. 2009; 324:768–771. [PubMed: 19423822]
30. Han MY, Ozyilmaz B, Zhang Y, Kim P. Energy band-gap engineering of graphene nanoribbons. Phys Rev Lett. 2007; 98:206805–2068808. [PubMed: 17677729]
31. Li X, Wang X, Zhang L, Lee S, Dai H. Chemically derived, ultrasmooth graphene nanoribbon semiconductors. Science. 2008; 319:1229–1232. [PubMed: 18218865]
32. Kobayashi T, Kimura N, Chi J, Hirata S, Hobara D. Channel-length-dependent field-effect mobility and carrier concentration of reduced graphene oxide thin-film transistors. Small. 2010; 6:1210–1215. [PubMed: 20449851]
33. Bai J, Zhong X, Jiang S, Huang Y, Duan X. Graphene nanomesh. Nat Nanotechnol. 2010; 5:190–194. [PubMed: 20154685]

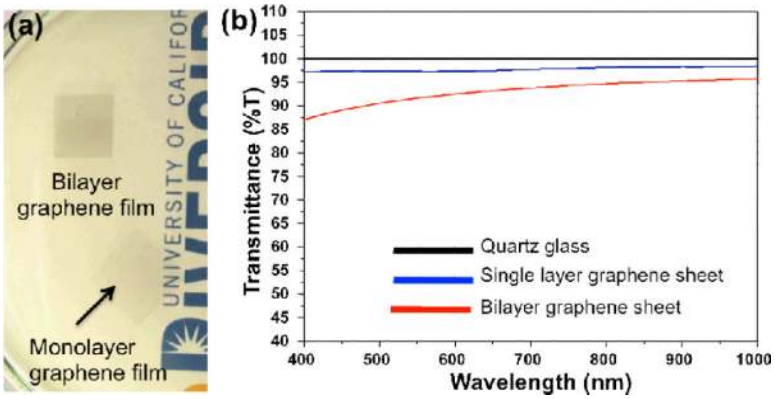

Fig. 1.

a) Optical micrograph showing single layer and bilayer graphene film synthesized at 900°C for 1 min using ethanol-CVD, floating on D.I. water. b) Optical transmittance of single and bilayer graphene films on a quartz substrate showing a transmittance value of about 97% and 91%, respectively, in the 500–**1000** nm wavelength regime.

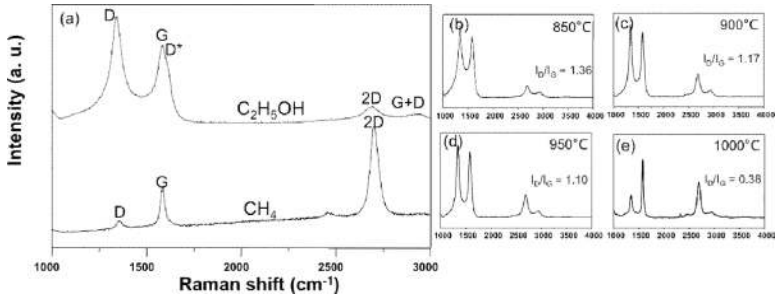

Fig. 2.

a) A comparison of collected Raman spectra of CVD grown graphene film synthesized at 900°C using CH_4 and C_2H_5OH precursors. b–e) Raman spectra of CVD grown graphene film grown for 1 min using ethanol vapor as a function of temperature.

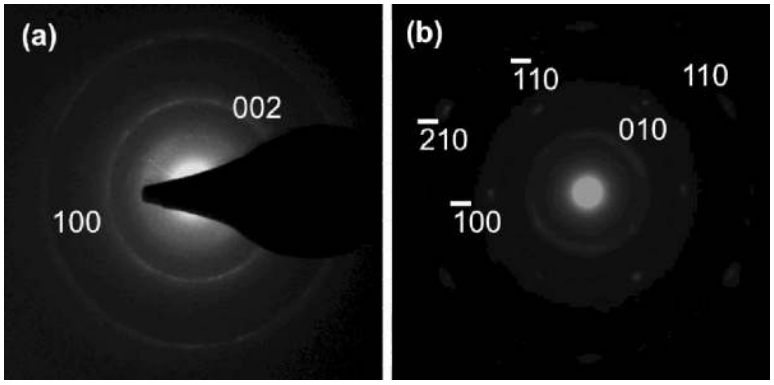

Fig. 3.
Electron diffraction pattern of CVD grown graphene film synthesized at 900°C using a) C_2H_5OH (for 1 min) and b) CH_4 (for 5 min) precursors.

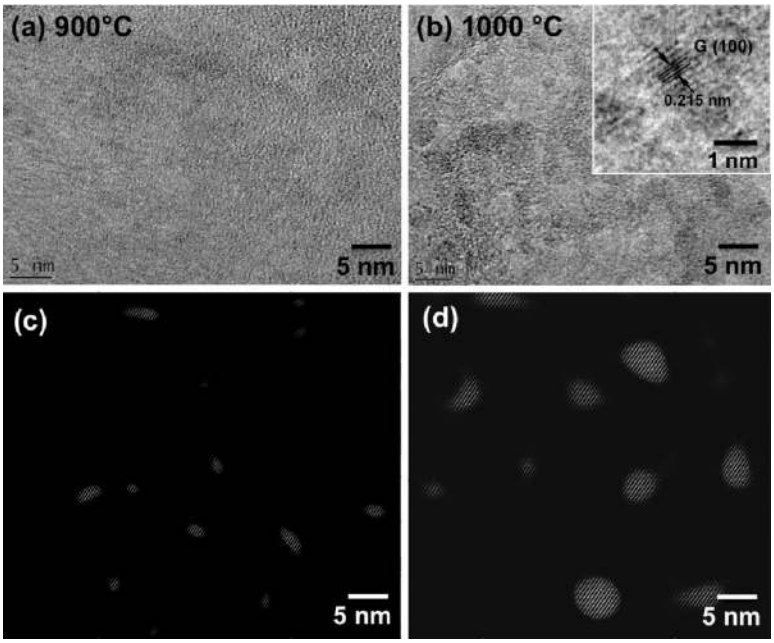

Fig. 4.
a, b) HRTEM and corresponding c, d) inverted FFT images of polycrystalline graphene film synthesized at 900°C and 1000°C using ethanol vapor.

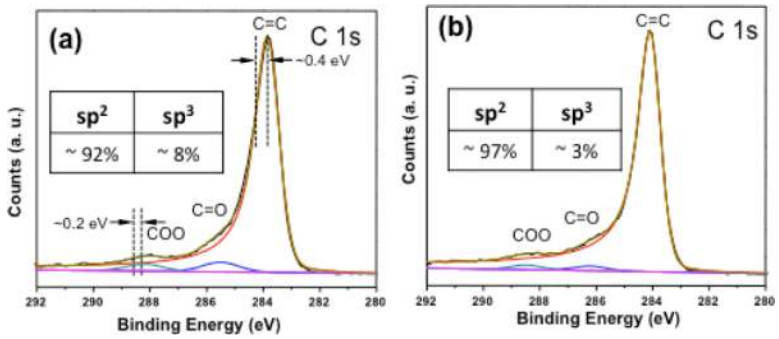

Fig. 5.

XPS spectra of ethanol CVD grown graphene film synthesized at a) 900°C and b) 1000°C for 1min using ethanol vapor.

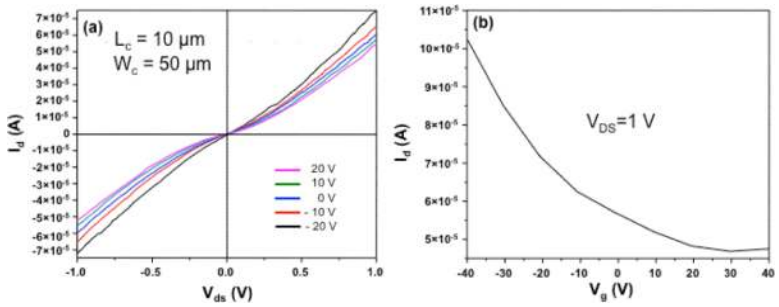

Fig. 6.

Electrical properties of polycrystalline graphene film synthesized at 900°C using ethanol vapor. a) Low bias two terminal source–drain current–voltage (I_d–V_{ds}) and b) transfer (I_d-V_g) characteristic curves recorded on a graphene FET (L_c=10 μm and W_c=50 μm).